RIS-Assisted Joint Preamble Detection and Localization

Nuti, Pooja; Kim, Kyeong Jin; Wang, Pu; Koike-Akino, Toshiaki; Parsons, Kieran

Abstract

Reconfigurable intelligent surface (RIS) is envisioned to be a key enabling technology for future wireless systems and is currently being developed and studied for various applications. In this work, we investigate how a single, passive RIS can assist both preamble detection and localization. We propose a joint preamble detection and localization scheme and a rule-based multi-antenna peak correction method to improve the reliability of range estimates and preamble detection. The proposed approach builds prior information on a low-speed factory vehicle's position based on a previously estimated position to more efficiently estimate the vehicle's current location along a trajectory. Simulation results present how RIS can enable these two tasks and how performance varies across various vehicle positions.

RIS-ASSISTED JOINT PREAMBLE DETECTION AND LOCALIZATION

Pooja Nuti[1,3]*, Kyeong Jin Kim*[2]*, Pu Wang*[1]*, Toshiaki Koike-Akino*[1]*, and Kieran Parsons*[1]

[1]Mitsubishi Electric Research Laboratories (MERL), Cambridge, MA 02139, USA
[2]Samsung Research America, Plano, TX 75023, USA
[3]The University of Texas at Austin, Austin, TX 78712, USA

ABSTRACT

Reconfigurable intelligent surface (RIS) is envisioned to be a key enabling technology for future wireless systems and is currently being developed and studied for various applications. In this work, we investigate how a single, passive RIS can assist both preamble detection and localization. We propose a joint preamble detection and localization scheme and a rule-based multi-antenna peak correction method to improve the reliability of range estimates and preamble detection. The proposed approach builds prior information on a low-speed factory vehicle's position based on a previously estimated position to more efficiently estimate the vehicle's current location along a trajectory. Simulation results present how RIS can enable these two tasks and how performance varies across various vehicle positions.

Index Terms— RIS, DoA estimation, ToA estimation, Peak correction, Statistical beamforming, RIS-aided localization.

1. INTRODUCTION

Future smart manufacturing demands connectivity of sensors, actuators, and controlling devices distributed across the factory while providing advanced localization services for factory vehicles such as an automated guided vehicle (AGV). Due to the ubiquitous presence of indoor Wi-Fi devices, Wi-Fi signals can be leveraged to localize indoor moving objects, even in non-line-of-sight (NLOS) scenarios. Wi-Fi-based localization can be categorized into range-based and range-free approaches [1]. Range-based approaches consist of measurements of time-difference-of-arrival (TDoA), time of arrival (ToA), and or angle of arrival (AoA) via triangulation techniques [1, 2]. Fingerprinting techniques can match either coarse-grained received signal strength indicator (RSSI), mid-grained beam training measurements, or fine-grained channel state measurements (CSI) to a radio map of the indoor space via data-driven approaches. Wi-Fi signals from different frequency bands can be combined to extract complementary features for robust localization [1–8].

In challenging scenarios, reconfigurable intelligent surfaces (RIS), a programmable metasurface comprised of a large number of low-cost, passive elements, can further assist Wi-Fi-based indoor localization by providing a means of controlling the wireless propagation environment. RIS-assisted localization has been studied in the literature [9–26]. In [27], an iterative positioning algorithm is proposed for beam training at terminals and AOA estimation. Cramer rao lower bound (CRLB) analysis on position and orientation of RIS is derived in [28]. RIS-aided downlink positioning is studied by Fisher information analysis and a two-step optimization is carried out to select the best active RIS subset to improve
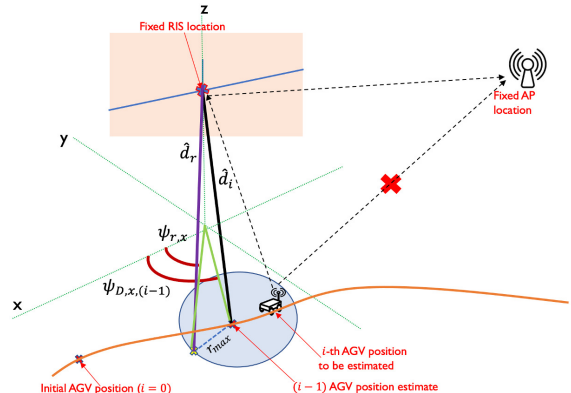
Fig. 1. An automated guided vehicle (AGV) travels along a trajectory and transmits Wi-Fi signals to an access point (AP) via an indirect path aided by reconfigurable intelligent surface (RIS).

positioning performance in [29]. In [16], CRLB is derived on the estimation error on channel parameters to to improve the LOS link through coherent combining and to solve a single-input single output (SISO) localization and synchronization problem. In [21], CRLB is derived for a radar target AoA within a joint sensing and waveform application. In [18], a two stage localization algorithm is proposed based on ToA and AoA estimation and prior statistical information on the UE position.

Most of the above RIS-assisted localization efforts have not exploited the Wi-Fi frame structure such as a preamble. A preamble is prepended to Wi-Fi packets to ensure that the receiver can detect the start of the frame and acquire initial synchronization [30]. In [31], preamble has been detection leveraged for range estimation in localization. In this paper, we propose to incorporate the frame structure for RIS-assisted joint preamble detection and localization. Specifically, our contributions are summarized as follows:

S1. We propose to build upon the work done in [18] by incorporating a WiFi-supported frame structure and extending the two-stage RIS-aided localization algorithm to support a low-mobility AGV by defining the prior information based on the knowledge on the previous position, as opposed to coarse assumed prior information.

S2. We propose a novel preamble detection algorithm with a rule-based multi-antenna peak correction stage in order to reduce false alarm detection and obtain a reliable ToA estimate. Employing available statistical knowledge of the training sequence such as periodicity and number of expected peaks to reconstruct the ideal cross-correlation signal, and utilizing receive diversity at the AP makes a key difference from the work of [30] and [31].

After analyzing the effect of the RIS on preamble detection when the RIS link between a transmitter and receiver serves as the only link available, we present numerical results to assess the performance of the proposed algorithm on localization.

2. SYSTEM MODEL

2.1. Geometry Model

As shown in Fig. 1, we consider a RIS-assisted millimeter-wave (mmWave) uplink communication system between a low-mobility AGV at $\mathbf{p}_{\text{UE}} = [x_{\text{UE}}, y_{\text{UE}}, z_{\text{UE}}]$ with a single antenna and a Wi-Fi access point (AP) with a uniform linear array (ULA) of M antennas at $\mathbf{p}_{\text{AP}} = [x_{\text{AP}}, y_{\text{AP}}, z_{\text{AP}}]$. We consider the case in which the direct path between the AGV and AP is fully blocked and only the AGV-RIS-AP uplink path is available. The RIS consists of N passive elements with tunable phase shifts $[0, 2\pi]$ modeled as a uniform planar array (UPA), where its reference center is located at $\mathbf{p}_{\text{R}} = [x_{\text{R}}, y_{\text{R}}, z_{\text{R}}]$.

The AGV-RIS link $\mathbf{h}(\mathbf{p}) \in \mathbb{C}^{N \times 1}$ and RIS-AP link $\mathbf{G} \in \mathbb{C}^{N \times M}$ are assumed to be Line-of-Sight (LOS) channels except that we also include the lognormal shadowing. Let $\theta = [\theta_{\text{x}}, \theta_{\text{z}}]$ be the AoA of the AGV-RIS path in azimuth and elevation. Then, AGV-RIS channel is given as

$$\mathbf{h}(\mathbf{p}) \triangleq \sqrt{\gamma} \mathbf{b}(\theta), \quad (1)$$

where $\gamma = \chi d^{-\beta}$ is the corresponding path loss with d denoting the unknown RIS-AGV distance and $\chi = 10^{0.1\phi_{\text{dB}}}$ modeling the lognormal shadowing via $\phi_{\text{dB}} \sim \mathcal{N}(0, \sigma_{\phi, \text{dB}}^2)$, and $\mathbf{b}(\theta) \in \mathbb{C}^{N \times 1}$ is the UPA array response array at the RIS

$$\mathbf{b}(\theta) = \mathbf{b}_{\text{y}}(\theta) \otimes \mathbf{b}_{\text{x}}(\theta), \quad (2)$$

with $\mathbf{b}_{\text{y}}(\theta)$ and $\mathbf{b}_{\text{x}}(\theta)$, respectively, defined as

$$\mathbf{b}_{\text{x}}(\theta) = [1, e^{j\delta' \cos\theta_{\text{x}} \sin\theta_{\text{z}}}, \ldots, e^{j\delta'(N_{\text{x}}-1)\cos\theta_{\text{x}} \sin\theta_{\text{z}}}]^{\text{T}},$$

$$\mathbf{b}_{\text{y}}(\theta) = [1, e^{j\delta' \sin\theta_{\text{x}} \sin\theta_{\text{z}}}, \ldots, e^{j\delta'(N_{\text{y}}-1)\sin\theta_{\text{x}} \sin\theta_{\text{z}}}]^{\text{T}},$$

with $N_{\text{x}} N_{\text{y}} = N$ and $\delta' = 2\pi\delta/\lambda$, where δ denotes the antenna spacing and λ the wavelength.

Denote $\psi_{\text{D}} = [\psi_{\text{D,x}}, \psi_{\text{D,z}}]$ as the angle of departure (AoD) from the RIS to the AP in azimuth and elevation and ψ_{A} to be the AoA at the AP. Then, the LOS RIS-AP channel is given by

$$\mathbf{G} \triangleq \sqrt{\gamma_{\text{G}}} \mathbf{b}(\psi_{\text{D}}) \mathbf{a}(\psi_{\text{A}})^{\text{H}}, \quad (3)$$

where the path loss term γ_{G} follows a similar form to that of the AGV-RIS link, i.e., $\gamma_{\text{G}} = \chi d_{\text{G}}^{-\beta}$ with d_{G} denoting the known RIS-AP distance, $\mathbf{b}(\psi_{\text{D}}) \in \mathbb{C}^{N \times 1}$ is the UPA array response as a function of the AoD ψ_{D} (similarly defined as (1) by changing the AoA θ to AoD ψ_{D}), and the ULA array response at the AP

$$\mathbf{a}(\psi_{\text{A}}) = [1, e^{j\delta' \sin(\psi_{\text{A}})}, \ldots, e^{j\delta'(M-1)\sin(\psi_{\text{A}})}]. \quad (4)$$

2.2. Signal Model

In this work, we consider a frame structure similar to that of the single-carrier physical layer frame of 802.11ad [32] which is compatible with wireless local access networks (WLANs) including Wi-Fi. More specifically, we focus on the short training field (STF) of the 802.11ad preamble to jointly carry out preamble detection and extract a distance measurement for localization. The STF is comprised of Q repetitions of 128-sample Golay complementary sequence Ga_{128} followed by its binary complement $-\text{Ga}_{128}$ [31, 33].

We assume a narrowband transmission and a moving AGV equipped with a single-antenna transmitting a preamble training sequence $s[k]$ where k denotes the time slot index. The received uplink AGV-RIS-AP signal is expressed as

$$\mathbf{y}[k] = \sqrt{P} \mathbf{G}^{\text{H}} \mathbf{\Phi}[k]^{\text{H}} \mathbf{h}(\mathbf{p}) s[k] + \mathbf{n}[k] \in \mathbb{C}^{M \times 1}, \quad (5)$$

where P is the transmit power of the AGV, $\mathbf{\Phi}[k]$ is a diagonal matrix containing the amplitude and phase shifts associated with each RIS element along the diagonal of form $\mathbf{\Phi}[k] = \text{diag}[\alpha_1[k]e^{j\phi_1[k]} \ldots \alpha_N[k]e^{j\phi_N[k]}]$, with $\phi_i[k] \in [0, 2\pi]$ and $|\alpha_i[k]|^2 \leq 1 \ \forall i$, and $\mathbf{n}[k] \in \mathbb{C}^{M \times 1} \sim \mathcal{CN}(0, \sigma_{\text{n}}^2 \mathbf{I})$ denotes an additive white Gaussian noise with zero mean and noise variance σ_{n}^2. Furthermore, amplitudes and phases in $\mathbf{\Phi}[k]$ are assumed to be independently optimized. The received SNR is defined below

$$\text{SNR}(\mathbf{p}, k) = P||\mathbf{G}^{\text{H}} \mathbf{\Phi}[k]^{\text{H}} \mathbf{h}(\mathbf{p})||^2 / \sigma^2. \quad (6)$$

which can be used for AoA estimation and RIS optimization.

3. JOINT PREAMBLE DETECTION AND LOCALIZATION

3.1. RIS-Assisted Preamble Detection

Preamble detection is an essential component during initial access. The first stage of our localization carries out preamble detection and range estimation using a cross-correlation based approach through the passive RIS link. We consider the cross-correlation between the received signal $\mathbf{y}[k]$ and known training sequence $p[k]$, which is given by $p[k] = \text{Ga}_{128}$. When $y_m[k]$ denotes the m-th element of $\mathbf{y}[k]$, the cross correlation for preamble detection is given by

$$R_m[l] = \sum_{k=0}^{K-1} y_m[k] p^*[k - l], 0 \leq m \leq M-1, 0 \leq l < L-1,$$

where l is the correlation lag index, $K = Q(128+1) + L_{\text{CP}}$ with L_{CP} denoting the cyclic prefix length. Due to the expected periodicity of $y_m[k]$, the first peak in the set of detected peaks corresponds to preamble detection peak l_{P} and is extracted from $R_m[l]$ using the following rule:

$$\hat{l}_m = \min\{l | |R_m[l]|/C_m \geq \mu\}, \forall l \quad (7)$$

where $C_m \triangleq \max\{R_m[l], \forall l\}$ and μ is a given threshold value less than 1. The delay corresponding to ToA is obtained from the preamble detection estimate as $\hat{l}_{\text{ToA}} = \hat{l}_m - L_{\text{CP}}$. Thus, the performance of peak detection via the RIS corresponds to the performance of ToA estimation and consequently directly impacts localization performance. In the lower SNR regime, peak detection based on μ becomes challenging as noise corrupts the cross-correlation output and peak detection becomes more susceptible to incorrect peak selection. Thus, we propose a peak correction algorithm to improve peak detection and eventually ToA estimation, in the low SNR regime, where an accurate estimate of noise floor may not be available. We note that even when the received signal can be filtered with respect to a noise floor, $R_m[l]$ may still contain spurious peaks.

3.2. Rule-based Multi-Antenna Peak Correction

Let $\mathbb{L}_m \triangleq \{[l_1]_m, [l_2]_m, \ldots, [l_Q]_m\}$ denote a set of peaks by applying the above peak detection to the mth antenna at AP, and its size is denoted by $\text{cal}(\mathbb{L}_m) = Q$. Owing to periodicity of the STF composed by $p[k]$, we have the following constraints for the cross-correlation peaks:

$$[l_{j\pm l}]_m - [l_j]_m = \pm 128l, \forall j \in \{1, \ldots, Q\} \text{ and } \forall m, \quad (8)$$

$$\text{cal}(\mathbb{L}_m) = Q, \forall m, \quad (9)$$

$$[l_1]_m \geq 0 \text{ and } [l_Q]_m \leq K, \forall m. \quad (10)$$

Note that (10) is a boundary condition to fix missing peaks in $\mathbb{L}_m$. At a given threshold μ, the peak detector may not satisfy constraint (9). Thus, using constraint (8), we first form a set of candidates $\mathbb{L}_m$.

Our rule-based multi-antenna peak correction follows rules corresponding to the above constraints of (8), (9), (10) and exploits the cross-correlation consistency over multiple antennas at the AP.

C1. **Rule-based Peak Correction**: From (8), missing but expected peaks between detected peaks are reinstated to a lag index that restores the periodic recurrence of cross-correlation peaks and is added to the detected peak set $\mathbb{L}_m$. If (9) is not satisfied even after applying this correction, we begin appending missing peaks to either the beginning or end of $\mathbb{L}_m$ sequentially. If a missing peak is found at a lag index greater than K, the length of the cross-correlation output, we reintroduce a missing peak at the beginning of $\mathbb{L}_m$ as long as the corresponding lag index is positive (see (10)) and the total number of peaks is not greater than Q (see (9)). If constraint (10) is not violated by either appending a peak at the beginning or end of the current peak sequence $\mathbb{L}_m$, the missing peak location is selected based on cross-correlation signal power. Missing peaks are sequentially added to $\mathbb{L}_m$ until (9) is met. Finally, denoting the updated peak set as $\tilde{\mathbb{L}}_m$, the ToA is estimated as the leading peak in $\tilde{\mathbb{L}}_m$ as

$$P_m = \tilde{\mathbb{L}}_m[0]. \qquad (11)$$

C2. **Multi-Antenna Peak Consistency**: Since the AP is equipped with M antennas, our peak correction further exploits the receiving antenna diversity to improve the reliability. Among M leading peaks $\{P_m\}_{m=1}^M$, we apply the majority rule as follows:

$$[C, \tilde{P}] = \text{Majority}(\{P_m, m = 1, \ldots, M\}), \qquad (12)$$

where C denotes the number of the most frequent leading peak $\tilde{P}$. In other words, we pick the most consistent ToA estimate across all M antennas. The larger C is, the more reliable $\tilde{P}$ is for the ToA estimate. Thus, receive diversity at the AP increases reliability in peak detection.

C3. **RIS-Assisted Peak Correction**: In scenarios (e.g., deep fading) that the majority rule fails (i.e., $C < \lfloor M/2 \rfloor$), it may imply that the corresponding RIS coefficients $\boldsymbol{\Phi}$ may not be ideal. In this case, we re-evaluate the peak detection with a new Gaussian randomization selection for the semidefinite program (SDP) optimization (see the subsection below), until the majority rule is met or a predefined number of attempts are met N_{D}.

Thus, the proposed peak correction can increase reliability of the preamble detection and ToA estimation.

3.3. RIS-Assisted Localization

We consider localization in the SIMO setting based on two angular measures and a range estimate. We denote the ToA estimate as $\hat{\tau}_{\text{TOA}}$, and obtain an estimate of the AGV-RIS distance as

$$\hat{d} = \hat{\tau}_{\text{TOA}} c - d_{\text{G}}. \qquad (13)$$

Then, assuming knowledge of the AGV height z_{UE}, an estimate of the elevation AoA is obtained as

$$\hat{\psi}_{\text{D,z}} = \arccos((z_{\text{RIS}} - z_{\text{UE}})/\hat{d}). \qquad (14)$$

Furthermore, for azimuth AoA estimate $\hat{\psi}_{\text{D,x}}$, we adopt a similar approach to the one in [18]. Nevertheless, the difference is that we estimate the range (3.1) prior to the azimuth angle estimation, thus reducing a two-dimensional search space to a one-dimensional search in the angular domain. The remaining search space is then again split into a predefined number of subareas N_{a} repetitively, and statistical beamforming is performed from each subregion. A distribution of

user locations $f_{\mathbf{P}}(\mathbf{p})$ is then generated from each subregion and the RIS is optimized with respect to the position that minimizes (6).

The initial position along a trajectory may correspond to a setting in which an AGV has lost direct communication with the AP and is switching to communication with the AP via the RIS. In such a setting that no recent CSI of $\mathbf{h}(\mathbf{p})$ is available to optimize the RIS, we measure the SNR of (6) by randomly choosing $\boldsymbol{a}_i$ and $\boldsymbol{g}_i$ out of a random codebook, and choose a pair of corresponding $\boldsymbol{a}_i$ and $\boldsymbol{g}_i$ that maximizes the SNR. Then, we can have

$$\boldsymbol{\Phi} = \text{diag}(\boldsymbol{a} \circ \exp(j\boldsymbol{g})), \qquad (15)$$

where $\circ$ denotes the Hadamard product.

In contrast, when channel estimates of $\mathbf{h}(\mathbf{p})$ from a previous position are available, a SDP as in [18] is applied as follows:

$$\max_{\mathbf{V} \succeq \mathbf{0}} \min_{\{\mathbf{p}_t\}_{t=1}^T} \text{tr}(\bar{\mathbf{H}}(\mathbf{p}_t)\mathbf{V}) \qquad (16)$$
$$\text{s.t.} \quad \text{diag}(\mathbf{V}) \leq 1, \quad \text{rank}(\mathbf{V}) = 1,$$

where T is the number of sample points drawn from $f_{\mathbf{P}}(\mathbf{p})$, $\mathbf{V} = \mathbf{v}\mathbf{v}^H$ with $\mathbf{v} = [\alpha_1 e^{-j\phi_1}, \cdots, \alpha_N e^{-j\phi_N}]^T$, and $\bar{\mathbf{H}}(\mathbf{p}_t) = \mathbf{H}(\mathbf{p}_t)\mathbf{H}(\mathbf{p}_t)^H$ where $\mathbf{H}(\mathbf{p}_t) = \text{diag}(\mathbf{h}(\mathbf{p}_t)^{\text{H}})\mathbf{G}$ such that the SNR of (6) can be written as a quadratic function $P\|\mathbf{v}^{\text{H}}\mathbf{H}(\mathbf{p})\|/\sigma^2$ which gives rise to the form in (16).

3.4. Overall Localization Algorithm

The overall localization algorithm is summarized as follows:

A1. The initial position uses a random codebook to optimize the RIS. Preamble detection and range estimation are then evaluated as defined in Section 3.1. An estimate of the elevation angle and range estimate is calculated. Azimuth AoA $\hat{\psi}_{\text{D,x}}$ is then calculated where the initial azimuth angle search space considered at the initial position along a trajectory is $[-\pi/2, \pi/2]$. The rectangular coordinate estimates of the AGV are then calculated and used to evaluate euclidean localization error:

$$\hat{x}(\mathbf{p}) = x_{\text{RIS}} - \hat{d}(\mathbf{p}) \sin(\hat{\psi}_{\text{D,z}}) \cos(\hat{\psi}_{\text{D,x}}),$$
$$\hat{y}(\mathbf{p}) = y_{\text{RIS}} - \hat{d}(\mathbf{p}) \sin(\hat{\psi}_{\text{D,z}}) \sin(\hat{\psi}_{\text{D,x}}). \qquad (17)$$

A2. In subsequent positions, the azimuth search space is defined based on the previous time step azimuth AoA estimate $\hat{\psi}_{\text{D,x,(i-1)}}$ and predefined radius as indicated in Fig. 1. We assume a maximum speed v that a user can move at and define a maximum radius $r_{\max} = v\tau$ a user could have moved from its current estimated position where τ is the assumed time difference between the previous $(i-1)$th position and current ith position. Knowing the position of the RIS and estimated location of the user, the minimum and maximum azimuth angles defining the search space for estimation of the current ith position are calculated using the azimuth difference Δ_{az}, i.e., $\Delta_{\text{az}} = |\hat{\psi}_{\text{D,x,(i-1)}} - \psi_{\text{r,x}}|$, where $\hat{\psi}_{\text{D,x}} = \arctan(\hat{y}(\mathbf{p})/\hat{x}(\mathbf{p}))$ and $\hat{\psi}_{\text{r,x}}$ is an azimuth angle corresponding to a location along the circumference of potential positions of the AGV at position i defined from the $(i-1)$th estimated position as $\hat{\psi}_{\text{r,x}} = \arctan(\hat{y}(\mathbf{p})/(\hat{x}(\mathbf{p}) - r_{\max}))$. Using a determined Δ_{az}, we define the azimuth search space for the ith position as $[\hat{\psi}_{\text{D,x,(i-1)}} - \Delta_{\text{az}}, \hat{\psi}_{\text{D,x,(i-1)}} + \Delta_{\text{az}}]$.

A3. The angular search space is split into N_{a} uniform subregions, in which a sample AGV location is randomly selected from the subregion. The RIS is then optimized by (16) and an estimate of $\hat{\psi}_{\text{D,x,(i)}}$ is retrieved from the subregion using MUSIC [18]. Received SNR is used to iteratively refine $\hat{\psi}_{\text{D,x,(i)}}$.
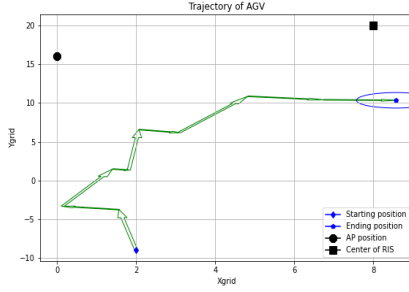
Fig. 2. 2D trajectory of AGV along factory floor

In future work, a multi-AGV setting can be supported by the proposed localization solution by incorporating a signal decoding stage to alleviate interference during preamble detection and optimizing the RIS based on the signal-to-interference-plus noise ratio. A trade-off between the number of users supported by a single RIS and localization error may exist.

4. NUMERICAL RESULTS

We evaluate localization error along a trajectory shown in Fig. 2 of a typical factory floor setting where the coordinates of AGV, RIS and AP are marked. The AGV moves closer to the AP and RIS over the course of the trajectory with varying distances to AP $d_{AP} \in [7, 25]$m and distances to RIS $d_{RIS} \in [10, 30]$m. We use the following parameters for the evaluation of the proposed algorithm: i) $M = 4$, $N \in \{16, 64, 144\}$; ii) AGV is equipped with a single antenna; iii) the elevation height info is assumed to be known and constant with $z_{RIS} = z_{AP} = 4$m and $z_{UE} = 2$m; iv) LOS channels are modeled with $\beta = 1.73$ and $\sigma^2_{\phi,dB} = 3.02$; v) transmit power at the AGV is 20 dBm; vi) sampling frequency is 60.72 MHz; vii) cross-correlation detection threshold $\mu = 0.65$ for the initial peak detection and $Q = 10$; viii) $N_a = 3$ in the AoA estimation, and no overlap is assumed between the subregions; and x) threshold for convergence between subsequent AoA estimates is set as $\epsilon = .05$ in degrees, ix) $N_D = 1000$ to manage the low SNR setting considered.

In Fig. 3, we illustrate an example of peak detection and correction at an SNR of 15 dB. The top plot clearly shows the challenges regarding correlation-based frame detection and the issue of false detected peaks even at a reasonable SNR range. With the rule-based multi-antenna peak correction, the corrected peak locations of $R_m[l]$
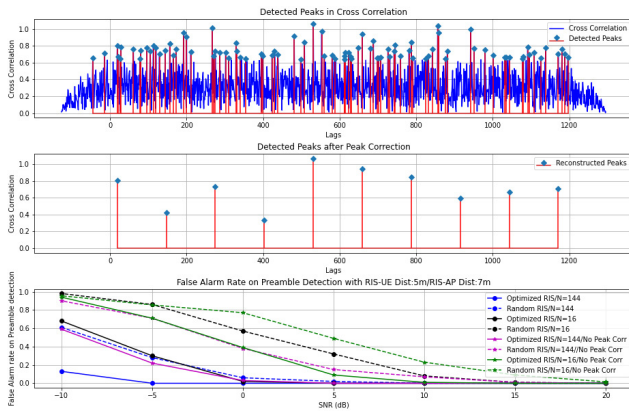

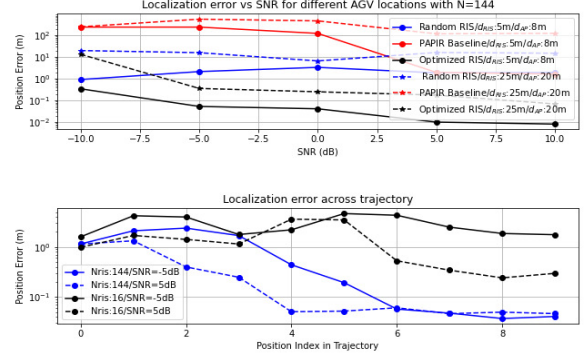**Fig. 3**. An example of preamble peak detection and correction.

Fig. 4. Localization error across trajectory provided in Fig. 2

are reconstructed as shown in the middle plot of Fig. 3, in which the preamble start is successfully located. The bottom plot further reveals that i) either an optimized RIS or a RIS with more elements reduces the false alarm rate. This is more evident at the lower SNR regime. Specifically at the SNR of -10 dB, the proposed approach with $N = 144$ RIS elements can reduce the false alarm rate from 0.98 to 0.16; and ii) make the false alarm rate less sensitive to the operating SNR.

The impact of an operating SNR is further investigated in the top plot of Fig. 4, where we present a performance comparison between the proposed approach with 1) a randomly configured RIS and 2) the PAPIR localization approach of [18]. It is noted that [18] assumes an SNR of 100 dB, a *known* AoA search space and known elevation angle, conducts AoA estimate over a wide search space, and relies on detection of a single peak corresponding to a ToA estimate, resulting in a large localization error. In [18], the range estimation is evaluated after AoA estimation. If there are substantial AoA estimation errors, the received signal is measured without a good RIS configuration and the sufficient beamforming gain of the RIS may not be achieved to compensate for the high noise level. In contrast, we utilize the beamforming gains of the RIS through evaluating ToA first with $\mathbf{\Phi}$ optimized via random codebook or with a recent $\mathbf{\Phi}$. Consequently, localization error is more robust to AoA errors in the proposed approach, as we can still reliably estimate the range as indicated in Fig. 4. The results presented in Fig. 4 serve as an upper bound on range estimation performance for position index i as $\mathbf{\Phi}$ is optimized according to estimated channel parameters of position $(i - 1)$. Fig. 4 shows that when N is small, e.g., $N = 16$, the position error does not converge as the position index increases. In contrast, when $N = 144$, the proposed approach yields converged position errors with less then 0.1m even at an SNR of -5 dB, and reduces the convergence time to achieve less than 10% of the position error of the initial position. Thus, it is necessary to employ sufficient passive elements according to the position of the AGV with respect to the AP and RIS to achieve reliable RIS-aided localization.

5. CONCLUSION

This paper has introduced a joint preamble detection and localization method to incorporate the frame structure for RIS-assisted Wi-Fi indoor localization. Specifically, for a low-speed AGV, previously estimated positions have been used to sequentially define prior knowledge for RIS-assisted localization, and ToA corrections to improve reliability of the preamble detection. Numerical results validate how exploiting a single, passive RIS can enable initial access procedures and localization across SNR and positions.

6. REFERENCES

[1] R. Zekavat and R. M. Buehrer, "Handbook of position location: Theory, practice and advances," 2011.

[2] N. Singh, S. Choe, and R. Punmiya, "Machine learning based indoor localization using Wi-Fi RSSI fingerprints: An overview," *IEEE Access*, vol. 9, pp. 127150–127174, 2021.

[3] M. Pajovic et al., "Fingerprinting-based indoor localization with commercial MMWave WiFi–Part I: RSS and Beam Indices," in *GLOBECOM*, Dec. 2019.

[4] P. Wang et al., "Fingerprinting-based indoor localization with commercial mmwave WiFi–Part II: Spatial beam SNRs," in *GLOBECOM*, Dec 2019.

[5] P. Wang, T. Koike-Akino, and P. V. Orlik, "Fingerprinting-based indoor localization with commercial MMWave WiFi: NLOS propagation," in *GLOBECOM*, 2020, pp. 1–6.

[6] T. Koike-Akino et al., "Fingerprinting-based indoor localization with commercial mmwave WiFi: A deep learning approach," *IEEE Access*, vol. 8, pp. 84879–84892, 2020.

[7] J. Yu et al., "Multi-band Wi-Fi sensing with matched feature granularity," *IEEE Internet of Things Journal*, pp. 1–1, 2022.

[8] C.J. Vaca-Rubio et al., "mmWave Wi-Fi trajectory estimation with continuous-time neural dynamic learning," in *ICASSP*, 2023, pp. 1–5.

[9] H. Wymeersch et al., "Radio localization and mapping with reconfigurable intelligent surfaces: Challenges, opportunities, and research directions," *IEEE Veh. Technol. Mag.*, vol. 15, no. 4, pp. 52–61, 2020.

[10] Z. Abu-Shaban et al., "Near-field localization with a reconfigurable intelligent surface acting as lens," in *Proc. IEEE Int. Conf. Commun.*, 2021, pp. 1–6.

[11] A. Fascista et al., "RIS-aided joint localization and synchronization with a single-antenna receiver: Beamforming design and low-complexity estimation," *IEEE J. Sel. Topics Signal Process.*, vol. 16, no. 5, pp. 1141–1156, 2022.

[12] E. Čišija et al., "RIS-aided mmWave MIMO radar system for adaptive multi-target localization," in *SSP*, 2021, pp. 196–200.

[13] Y. Liu, E. Liu, R. Wang, and Y. Geng, "Reconfigurable intelligent surface aided localization," in *Proc. IEEE Int. Conf. Commun.*, 2021, pp. 1–6.

[14] F. Guidi and D. Dardari, "Radio positioning with EM processing of the spherical wavefront," *IEEE Trans. Wireless Commun.*, vol. 20, no. 6, pp. 3571–3586, 2021.

[15] G. C. Alexandropoulos, I. Vinieratou, and H. Wymeersch, "Localization via multiple reconfigurable intelligent surfaces equipped with single receive RF chains," *IEEE Wireless Commun. Lett.*, vol. 11, no. 5, pp. 1072–1076, 2022.

[16] K. Keykhosravi et al., "SISO RIS-enabled joint 3D downlink localization and synchronization," in *ICC*, 2021, pp. 1–6.

[17] B. Luo et al., "Reconfigurable intelligent surface assisted millimeter wave indoor localization systems," in *Proc. IEEE Int. Conf. Commun.*, 2022, pp. 4535–4540.

[18] A. Albanese, P. Mursia, V. Sciancalepore, and X. Costa-Pérez, "PAPIR: Practical RIS-aided localization via statistical user information," in *IEEE Int. Workshop on Signal Process. Advances in Wireless Commun. (SPAWC)*, 2021, pp. 531–535.

[19] T. Ma, Y. Xiao, X. Lei, W. Xiong, and Y. Ding, "Indoor localization with reconfigurable intelligent surface," *IEEE Commun. Lett.*, vol. 25, no. 1, pp. 161–165, 2021.

[20] D. Dardari et al., "LOS/NLOS near-field localization with a large reconfigurable intelligent surface," *IEEE Trans. Wireless Commun.*, vol. 21, no. 6, pp. 4282–4294, 2022.

[21] Z. Esmaeilbeig et al., "Joint waveform and passive beamformer design in multi-IRS-aided radar," in *IEEE Int. Conf. on Acoustics, Speech and Signal Processing (ICASSP)*, 2023, pp. 1–5.

[22] Z. Yu et al., "Location sensing and beamforming design for IRS-enabled multi-user ISAC systems," *IEEE Trans. on Signal Process.*, vol. 70, pp. 5178–5193, 2022.

[23] A. Elzanaty et al., "Reconfigurable intelligent surfaces for localization: Position and orientation error bounds," *IEEE Trans. Signal Process.*, vol. 69, pp. 5386–5402, 2021.

[24] H. Zhang et al., "Towards ubiquitous positioning by leveraging reconfigurable intelligent surface," *IEEE Commun. Lett.*, vol. 25, no. 1, pp. 284–288, 2021.

[25] Z. Wang et al., "Location awareness in beyond 5G networks via reconfigurable intelligent surfaces," *IEEE Journal on Sel. Areas in Commun.*, vol. 40, no. 7, pp. 2011–2025, 2022.

[26] E. Björnson et al., "Reconfigurable intelligent surfaces: A signal processing perspective with wireless applications," *IEEE Sig. Process. Mag.*, vol. 39, no. 2, pp. 135–158, 2022.

[27] W. Wang and W. Zhang, "Joint beam training and positioning for intelligent reflecting surfaces assisted millimeter wave communications," *IEEE Trans. Wireless Commun.*, vol. 20, no. 10, pp. 6282–6297, 2021.

[28] S. Hu, F. Rusek, and O. Edfors, "Beyond massive MIMO: The potential of positioning with large intelligent surfaces," *IEEE Trans. Signal Process.*, vol. 66, no. 7, pp. 1761–1774, 2018.

[29] J. He et al., "Beyond 5G RIS mmWave systems: Where communication and localization meet," *IEEE Access*, vol. 10, pp. 68075–68084, 2022.

[30] V. Ninkovic et al., "Preamble-based packet detection in Wi-Fi: A deep learning approach," in *VTC-Fall*, 2020, pp. 1–5.

[31] P. Kumari, J. Choi, N. González-Prelcic, and R. W. Heath, "IEEE 802.11ad-based radar: An approach to joint vehicular communication-radar system," *IEEE Trans. Veh. Technol.*, vol. 67, no. 4, pp. 3012–3027, 2018.

[32] *Wireless LAN Medium Access Control (MAC) and Physical Layer (PHY) Specifications: Enhancements for Very High Throughput in the 60GHz Band*, IEEE Std. 802.11ad, Mar. 2012.

[33] W. Liu et al., "All-digital synchronization for SC/OFDM mode of IEEE 802.15.3c and IEEE 802.11ad," *IEEE Trans. Circuits Syst. I*, vol. 62, no. 2, pp. 545–553, 2015.